Electrocatalytic enhancement of CO methanation at the metal-electrolyte interface studied by *in situ* X-ray photoelectron spectroscopy

Thurner Christoph W.[1†], Haug Leander[1†], Winkler Daniel[1†], Griesser Christoph[1], Leitner Matthias[1], Moser Toni[1], Werner Daniel[1], Thaler Marco[1], Scheibel Lucas A.[1], Götsch Thomas[2], Carbonio Emilia[2,3], Kunze-Liebhäuser Julia[1], Portenkirchner Engelbert[1], Penner Simon[1] and Klötzer Bernhard[1, z]

[1]*Institute of Physical Chemistry, University of Innsbruck, Innrain 52c, A-6020 Innsbruck, Austria*

[2] *Fritz-Haber Institute of the Max-Planck Society, Department of Inorganic Chemistry, Faradayweg 4–6, 14195 Berlin, Germany*

[3]*Catalysis for Energy, Energy Materials In-situ Laboratory (EMIL), Helmholtz-Zentrum Berlin für Materialien und Energie GmbH, BESSY II, Albert-Einstein-Straße 15, 12489 Berlin, Germany*

[†] C. T., L. H. and D. W. contributed equally and share first authorship

[z] Corresponding Author: [E-mail: bernhard.kloetzer@uibk.ac.at]

Abstract: For the direct reduction of CO_2 and H_2O in solid oxide electrolysis cells (SOECs) with cermet electrodes toward methane, a fundamental understanding of the role of elemental carbon as a key intermediate within the reaction pathway is of eminent interest. The present synchrotron-based *in situ* near-ambient-pressure X-ray photoelectron spectroscopy (NAP-XPS) study shows that alloying of Ni/yttria-stabilized-zirconia (YSZ) cermet electrodes with Cu can be used to control the electrochemical accumulation of interfacial carbon, and to optimize its reactivity toward CO_2. In the presence of syngas, sufficiently high cathodic potentials induce excess methane on the

studied Ni/yttria stabilized zirconia (YSZ)-, NiCu/YSZ- and Pt/gadolinium doped ceria (GDC) cermet systems. The hydrogenation of carbon, resulting from CO activation at the triple-phase boundary of Pt/GDC, is most efficient.

The co-electrolysis of CO_2(g) and water to methane (reaction 1) in high-temperature SOECs is a subject of mitigating issues related to climate change by utilizing the main greenhouse gas for electric energy storage in the form of a renewable energy carrier[1]:

$$CO_2 + 2H_2O \rightleftharpoons CH_4 + 2O_2 \quad (1)$$

The most common reaction pathway does not realize reaction (1) directly, as it deals with the simultaneous electrochemical reduction of CO_2 to CO and H_2O to H_2. The resulting CO/H_2 syngas mixture can be utilized to form a variety of hydrocarbons. For this, an adjustable CO/H_2 ratio is required, e.g. 1:3 to form methane (reaction 2).

$$CO + 3H_2 \rightleftharpoons CH_4 + H_2O \quad (2)$$

Based on thermodynamics, temperatures up to ~673 K are beneficial for CO methanation[2]. In this study we (i) provide a proof-of-principle that reactive carbon species are formed particularly on Ni(Cu)/8 mol% yttria stabilized-zirconia (8-YSZ) cermets via electrolysis of CO, and (ii) show that additional methane is formed generally on metal-electrolyte interfaces such as Ni(Cu)/8-YSZ and Pt/10 mol% Gd-doped ceria (GDC-10) even at high temperatures (~973 K) via electrocatalytic promotion of CO methanation. If an additional non-faradaic nature (i.e., change in the metal's work function and adsorbate chemistry) of the reaction, according to the concept of "electrochemical promotion of catalysis" (EPOC) or "non-faradaic electrochemical modification of catalytic activity" (NEMCA)[3], is present or not remains open.

In the co-electrolysis of CO_2 and H_2O, surface carbon chemistry plays a major role. Carbon can be deposited via different pathways, involving electrochemical (reaction (3)) or conventional

thermal reduction of CO (reaction (4), Boudouard reaction (5)). Commonly, these pathways are held responsible for surface coking and blocking of the triple-phase-boundary (TPB)[4].

$$CO + 2e^- \rightleftharpoons C + O^{2-} \quad (3)$$

$$CO + H_2 \rightleftharpoons C + H_2O \quad (4)$$

$$2CO \rightleftharpoons C + CO_2 \quad (5)$$

Vice versa, de-coking can proceed via the inverse reactions of (3,4,5) or, alternatively, via the reaction of carbon with co-generated hydrogen from electrochemical water splitting to form methane (reverse CH_4 pyrolysis reaction (6)):

$$C + 2H_2 \rightleftharpoons CH_4 \quad (6)$$

It is crucial for both, the efficiency of de-coking and of direct hydrocarbon formation, how reactive the material- and site-specific deposited carbon species are. In other words, equilibrium (6) imposes the need for a distinction between reactive *intermediate* and site-blocking *side product* carbon forms[5]. The carbon reactivity argument holds equally for the reversal of reaction (1), which needs to be realized for direct methane SOFCs[6].

For the electrochemical promotion of CH_4 synthesis according to reaction (2), both the kinetic reactivity and the chemical potential of carbon formed directly at the TPB via reaction (3) are essential. Electrode materials, which allow for modulation of the bond strength of this TPB-generated carbon, denoted as C_{TPB} in the following, are the key toward a knowledge-based reactivity control. Ni_xCu_y is considered as a promising alloy, fulfilling these carbon-chemistry related requirements[7]. Moreover, it features decreased carbon solubility, which is essential for the suppression of unreactive graphene/graphitic deposits[8, 9]. However, considering the thermo-catalytic methanation reaction of CO or CO_2, NiCu-alloyed catalysts perform worse than Ni[10, 11]. Nonetheless, it is important to note that alongside the hydrogenation of intermediate C, the rate-limiting step is the dissociation of CO or CO_2[12]. Anyway, the latter can be promoted by means of

electrochemistry (reaction (3)). As a result, it enables the utilization of electrocatalyst materials beyond the current scientific boundaries.

Taking the thermodynamic equilibrium constant K of reaction (6) into account, the carbon activity $a(C)$ influences the equilibrium pressure p of CH_4:

$$K = \frac{p(CH_4)}{a(C)\cdot p(H_2)^2} \qquad (7)$$

If additional carbon is induced electrochemically via reaction (3) in a H_2-containing atmosphere, the methane yield can be enhanced both by increasing the carbon activity via increasing the cathodic polarization, and by increasing the H_2 pressure[13]. Of course, the efficiency of the latter in terms of thermodynamic promotion of CH_4 yield, is limited by the kinetics of the reaction (6). In the following, a comparative approach, with respect to the C_{TPB} growth and clean-off on Ni/8-YSZ vs. $Ni_{80}Cu_{20}$/8-YSZ working electrodes (WE) and the C_{TPB}-promoted formation of methane on Ni(Cu)/8-YSZ (WE) vs. Pt/GDC-10 counter electrode (CE), is presented. This specifically designed CE is electrocatalytically highly active, featuring high surface area and an optimized number of TPB sites to minimize its overpotential contribution relative to the WE to negligible values[14]. The investigation of the interfacial carbon chemistry at defined atmospheres over cermet WEs was carried out via *in situ* near-ambient-pressure X-ray photoelectron spectroscopy (NAP-XPS) at the ISISS end station at the BESSY II synchrotron facility.

(i) Carbon-active electrodes

To highlight the difference in the carbon reactivity at the interface, visible in the kinetics of carbon growth and clean-off reactions, *in situ* XP spectra of the C 1s region of the Ni/8-YSZ and $Ni_{80}Cu_{20}$/8-YSZ electrodes were recorded at 973 K (Figure 1). In the order of the spectra from bottom to top, we applied initially 0.5 mbar CO at open circuit potential (OCP) to the electrode and detected a minor amount of mixed carbon-oxygenates and elemental carbon species in the C1s region (i.e., components are assigned to O-C=O_{ads}, C=O_{ads}, C-O-C_{ads} and C-C_{ads} species[15]). As the

Boudouard reaction (5) is strongly shifted toward CO formation under the chosen experimental conditions, we observed hardly any growth of the C1s signals after 15 min of isothermal exposure. Upon applying a voltage of -1.5 V, graphitic-like C_{TPB} at a BE of 284.7 eV can be electrochemically grown via reaction (3). After 15 min of CO electrolysis, the C_{TPB} growth was terminated by returning to OCP and CO pump-off. To study the efficiency of the oxidative clean-off reaction of this carbon species (reversal of reaction (5)), the electrode was then exposed to 0.13 mbar pure CO_2 under OCP conditions. For Ni/8-YSZ (left panel in Figure 1), only a slow decrease of the C_{TPB} component to ~87% of the initial value was observed after 5 min exposure. By increasing the CO_2 partial pressure up to 0.19 mbar and an exposure for additional 5 min, a further, but still rather slow decrease of the C_{TBP} peak area to ~58% of the initial value was achieved.

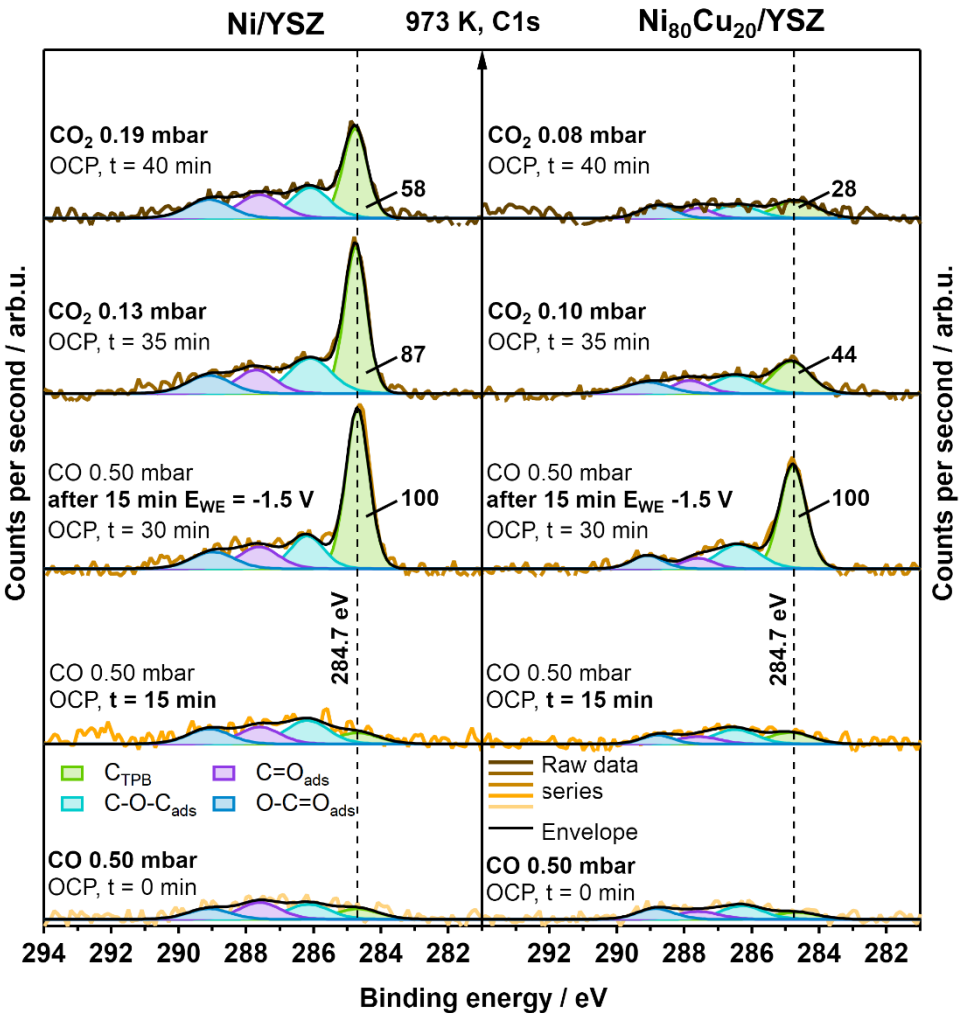

Figure 1. *In situ* XP spectra series of the C 1s region recorded on the Ni/8-YSZ and $Ni_{80}Cu_{20}$/8-YSZ WE at 973 K under the following conditions (from bottom to top): (a) 0.500 mbar CO, OCP (b) 0.500 mbar CO, OCP, after 15 min (c) 0.500 mbar CO, OCP, after 15 min -1.5 V (d) 0.13 mbar CO_2 for Ni/8-YSZ and 0.10 mbar CO_2 for $Ni_{80}Cu_{20}$/8-YSZ, both at OCP (e) 0.19 mbar CO_2 and 0.08 mbar CO_2 for the respective electrode.

In contrast, the amount of analogously grown C_{TPB} on the $Ni_{80}Cu_{20}$/8-YSZ electrode (right side in Figure 1) is diminished to ~44% already at a CO_2 pressure of 0.10 mbar after 5 min. After another 5 min (topmost spectra), the C_{TPB} peak started to vanish (i.e., 28% residual intensity),

although the CO_2 partial pressure was kept at an even lower value of 0.08 mbar. These results indicate that C_{TPB} is more reactive on the $Ni_{80}Cu_{20}$/8-YSZ electrode, at least for the oxidative carbon clean-off reaction (5). To confirm that carbon is accumulated via the TPB onto the cermet surface a XP spectra series (Figure S1) of Cu 2p Ni 2p, C 1s and Zr 3d were recorded before and after electrochemically induced carbon growth, showing a decrease in the cermet components. The Ni/Cu ratio in S1 changes from 2.95 before carbon growth toward 5.40 after. If this change is a consequence of the known alteration in the Ni to Cu surface composition upon electrochemically induced adsorbate chemistry[16] or if it is geometrically effect due to carbon growth on a porous electrode shielding Cu/Ni areas differently or if it arises from a carbon growths predominantly localized on Ni sites remains open.

To elucidate the C_{TPB} reactivity toward H_2 on Ni/8-YSZ and $Ni_{80}Cu_{20}$/8-YSZ, the reaction mixture was changed to 0.125 mbar CO and 0.375 mbar H_2 (total pressure 0.5 mbar; CO:H_2 ratio = 1:3). The XP spectra of the C1s region shown in Figure 2, recorded *in situ* at 973 K, show no carbon growth at open-circuit-potential (OCP). After applying a cathodic potential of -1.0 V for 30 min on either system, a graphitic-like C_{TPB}-related peak appears only on the $Ni_{80}Cu_{20}$/8-YSZ electrode (BE ≈284.7 eV). According to pronounced differences regarding carbon reactivity and bulk solubility on NiCu vs. pure Ni[8], we interpret this result in terms of hampered anti-segregation especially of C_{TPB} and its clean-off with H_2 (reaction (6)) on NiCu vs. Ni[11], leading to the accumulation of carbon at the surface. This raises the question whether this additional carbon species is kinetically available at all for enhanced methane formation through reaction (6). Equilibrium thermodynamics generally favor the reversal of (6) at increasing temperatures[2], but can be counteracted by the law of mass action (7), which predicts increasing methane pressures with increasing carbon activity *a(C)*. In turn, *a(C)* can be varied via polarization through equilibrium (3). Figure S2 in the supporting information provides the respective calculated equilibrium partial pressures of CH_4 at 973 K as a function of *a(C)*, based on data from[17].

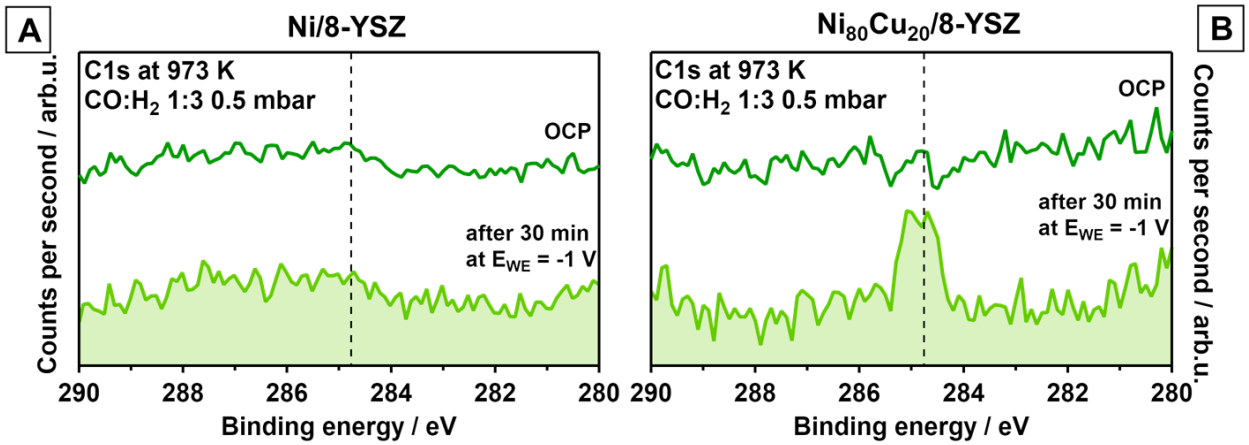

Figure 2. C1s XP-spectra recorded *in situ* at 973 K in 0.500 mbar $CO:H_2$ = 1:3 atmosphere at t = 0 s at OCP and after -1.0 V applied to the working electrode for 30 min (dark and light green traces, respectively). Panel A and B compare electrochemically induced C_{TBP} growth on Ni/8-YSZ vs. $Ni_{80}Cu_{20}$/8-YSZ (vertical dashed line).

(ii) Electrochemically promoted methane formation

In principle, the promotion of *a(C)* through reaction (3) via cathodic polarization can increase CH_4 formation thermodynamically through equilibrium (7). Whether the kinetics are in favor of a faster methanation, depends on the reactivity of the specific TPB sites, the H_2-reducibility of the electrolytically generated carbonaceous species, and the prevailing EPOC effect at the metal.

Cyclo-voltammetry (CV) combined with quadrupol mass spectrometry (QMS) allows to monitor methane formation on-line under high temperature conditions (973 K, Figure 3). The bottom region of Figure 3 represents the chosen sequence of linear sweeps of the potential (E_{WE}, scan rate = 50 mV/s, blue trace) and the resulting current (I, pink trace) as a function of time. As the SOEC is operated in a single reactant gas atmosphere (i.e., no separated anode and cathode compartments), the QMS detects gaseous species produced by both electrode sides, which makes a distinction between products formed at the WE vs. CE necessary (anode reactions: CO or H_2 oxidation). The potential was swept between -4 V and +4 V to generate high current densities and

thus, appropriate quantities of products for the QMS detection both at the $Ni_{80}Cu_{20}$/8-YSZ WE and the Pt/GDC-10 CE (Figure 3B). In panel A, the CV sweeps were limited to a strong cathodic polarization of the WE only, in order to suppress superimposed QMS intensity via cathodic polarization of the CE. The time-dependent intensity changes of the CH_4-specific (m/z = 15) signal measured during the sweeps can be directly correlated to the alternating potentials applied to the WE/CE (violet shaded area for the CE) and the respective electrolysis current changes. For details regarding QMS data analysis and I vs. E curves we refer to the SI (Figure S3).

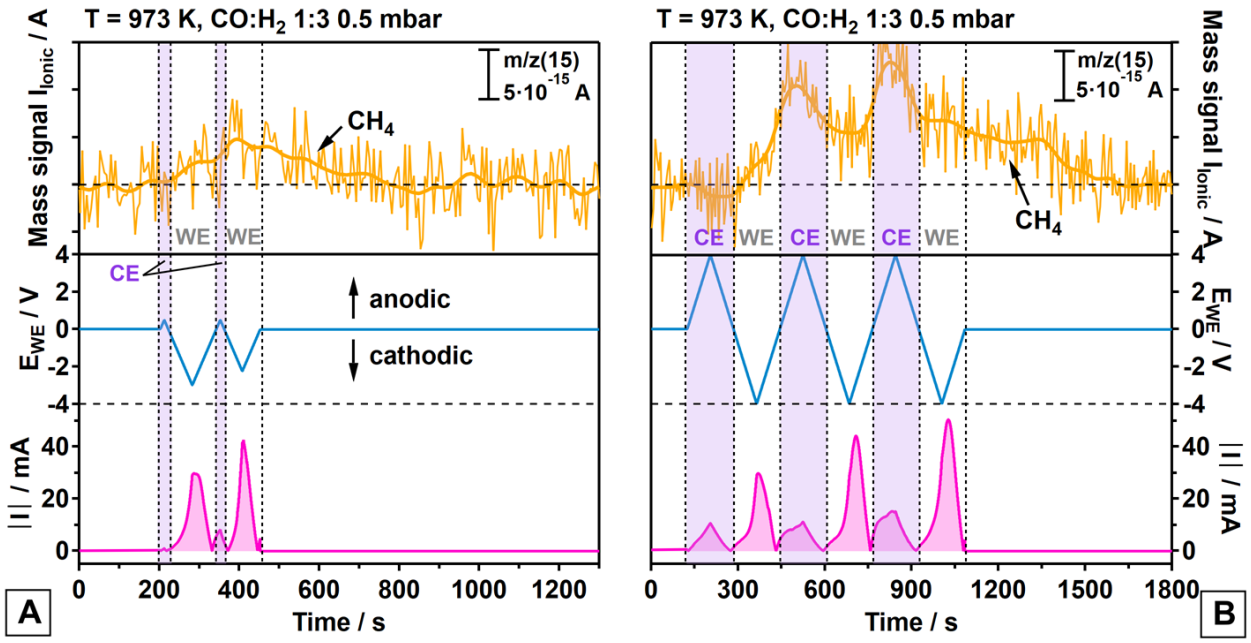

Figure 3. Top panels, light orange traces (raw and smoothed experimental data): electrochemically promoted methane formation caused by alternating the cathodic polarizations of the WE vs. CE. A: light blue traces: preferential cathodic polarization of $Ni_{80}Cu_{20}$/8-YSZ WE with max. 3V; B: alternating polarization of WE and CE with max. 4V. The respective absolute current changes are shown in the bottom panels as pink traces. To highlight the alternating cathodic operation of the CE vs. WE and the time-correlated changes of the m/z=15 mass signal of CH_4, negative potentials at the CE are highlighted by a violet-shaded background.

The main results derived from the data of Figure 3 are: 1) on both, the WE and the CE, the methanation reaction is promoted via cathodic polarization; 2) ongoing reaction (6) suggests the contribution of a faradaic enhancement in activity on both electrodes; 3) methane formation is much more promoted on the Pt/GDC-10 CE than on the WE, irrespective of Ni or $Ni_{80}Cu_{20}$ used as the metallic WE phase; 3) methane promotion at the CE is associated with a much smaller charge transfer for the CO electrolysis reaction (3) as compared to the WE, suggesting a relatively strong EPOC contribution on Pt/GDC; 4) the first cathodic polarization cycle of the CE yield no measurable CH_4 formation, but is expected to activate the CE for CH_4 formation for the second cycle; 5) once the CE is activated, the time-response of formation of additional CH_4 from C_{TPB} is much faster on the CE, as deduced from the synchronicity of cathodic WE polarization and the accelerated CH_4 increase; 6) CH_4 formation on the WE starts immediately in the beginning of the first cathodic polarization cycle, but then increases rather slowly and is associated with a smaller amount of CH_4 yielded from C_{TPB}, especially in view of the much larger integral charge transfer. The response of CH_4 formation to the alternating potential is very sluggish on the WE as compared to the CE.

In summary, the oxidative de-coking reaction of pre-deposited C_{TPB} in the presence of CO_2 ($C_{TPB} + CO_2 \rightarrow 2\ CO$) works more efficiently on $Ni_{80}Cu_{20}$, supporting its previously reported, enhanced coking resilience in the presence of CO_2 relative to clean Ni[8].

In contrast, the CO methanation results suggest that more C_{TPB} must have been formed electrochemically on $Ni_{80}Cu_{20}$/8-YSZ than on Pt/GDC-10, but remains kinetically less reactive toward methane formation. Considering the strongly different properties of the WE and CE materials, it appears reasonable that for both, less C_{TPB} accumulates on Pt in the presence of H_2, as carbon is weaker bonded and thus more reactive on Pt relative to Ni, and a more pronounced EPOC effect prevails on Pt. Moreover, H_2 activation is highly efficient on the carbon-free Pt surface. The

fact that the onset of CH_4 formation is hardly delayed on the WE, but needs a full cathodic activation cycle on the CE, can be explained by the much higher oxygen exchange capacity of GDC in comparison to 8-YSZ. Whereas any oxygen vacancy in 8-YSZ generated electrochemically at the WE side is immediately quenched by splitting of CO toward lattice oxygen and C_{TPB}, GDC likely requires an enhanced reductive activation by withdrawing sufficient lattice oxygen before CO can become dissociated at the TPB.

Unfortunately, the original goal of this study, namely the quantitative distinction of the electrochemical enhancement on CO-methanation on clean Ni vs. $Ni_{80}Cu_{20}$, is not sufficiently reliable in view of the signal-to-noise ratio of the available QMS data. Ni/8-YSZ and $Ni_{80}Cu_{20}$/8-YSZ show almost indistinguishable CH_4 formation properties, as shown in Figure S4 of the SI. These *operando* XPS measurements validate the accumulation of additional C_{TPB} only on $Ni_{80}Cu_{20}$/8-YSZ during the chronoamperometric experiments in a CO/H_2 atmosphere at -1.25 V, whereas on Ni/8-YSZ no C_{TPB} is visible at -1.00 V. However, the methane QMS signal (m/z = 15) increases similarly on both electrodes until the polarization is turned off. Figure S5 and S6 provides evidence of the metallic state of Ni and Cu anticipated under reductive CO/H_2 conditions. Together with the O1s region, no significant changes in the XP-spectra upon polarization (OCP vs. -1.25 V) were detected. Basically, one would expect NiCu to be a poorer thermal/non-electrochemical CO and/or CO_2 methanation catalyst than pure Ni[10, 11], but it remains unclear whether the proposed combination of faradaic and non-faradaic (EPOC) promotional effects can revert this trend. The preferential coking of NiCu under cathodic polarization in CO/H_2 may rather represent a hint for a delayed reaction of C_{TPB} toward CH_4, suggesting that NiCu may offer little, if any, advantages relative to pure Ni. If the electrochemically induced adsorbate and carbon chemistry affects the Cu/Ni segregation behavior and therefore alter gas surface interaction[16] remains open and calls for non-porous model electrode systems.

Nevertheless, the remaining central message of this work refers to the appropriate choice of materials to create a (bi)metal – mixed oxide electrolyte interface for optimized thermodynamic enhancement of CH_4 yiel with cathodically promoted kinetic EPOC action. The combination of activated bound carbon and hydrogen on the metallic component with superior properties of the metal-electrolyte interface for C-O bond activation is the key for electrochemical enhancement of the CH_4 yield in the co-electrolysis of CO_2 and water via intermediate CO and H_2. Obviously, these preconditions are rather matched by Pt/GDC than by Ni(Cu)/YSZ.

Experimental Methods

For cell preparation, sample mounting, equipment and XPS data analysis we refer to the supporting information (Figure S7).

Supporting Information

XPS comparison of Ni/8-YSZ vs. $Ni_{80}Cu_{20}$/8-YSZ upon carbon accumulation, Thermodynamic promotion of CH_4 formation, QMS data analysis and Cyclovoltammetry I vs. E curves, *Operando* XPS comparison of Ni/8-YSZ vs. $Ni_{80}Cu_{20}$/8-YSZ in CO/H_2 atmosphere, SOEC cell preparation, sample mounting, equipment and XPS data analysis

Acknowledgments

Financial support was provided by the research platform “Materials- and Nanoscience” and the special PhD program “Reactivity and Catalysis” at the University of Innsbruck. C. W. T. acknowledges a PhD position via doctoral program “Reactivity and Catalysis” of the University of Innsbruck. Additionally, L.H. and C.G. acknowledge funding by the Austrian Research Promotion Agency (FFG) via project 870523, and D. W. is a recipient of a DOC Fellowship of the Austrian

Academy of Sciences at the Department of Physical Chemistry. The Helmholtz Zentrum Berlin für Materialien und Energie, BESSY II, is acknowledged for the allocation of the beamtime to proposal number 202-09705-ST-1.1-P. E.P. acknowledge funding by the Austrian Research Promotion Agency (FFG) via project 877095 and by the Austrian Science Fund (FWF) via project P34233 and P35510.

References

(1) Zheng, Y.; Wang, J.; Yu, B.; Zhang, W.; Chen, J.; Qiao, J.; Zhang, J. A review of high temperature co-electrolysis of H_2O and CO_2 to produce sustainable fuels using solid oxide electrolysis cells (SOECs): advanced materials and technology. *Chem. Soc. Rev.* **2017**, *46* (5), 1427-1463. DOI: 10.1039/C6CS00403B.

(2) Gao, J.; Wang, Y.; Ping, Y.; Hu, D.; Xu, G.; Gu, F.; Su, F. A thermodynamic analysis of methanation reactions of carbon oxides for the production of synthetic natural gas. *RSC Advances* **2012**, *2* (6), 2358-2368. DOI: 10.1039/C2RA00632D.

(3) Vayenas, C. G.; Bebelis, S.; Neophytides, S. Non-Faradaic electrochemical modification of catalytic activity. *J. Phys. Chem.* **1988**, *92* (18), 5083-5085. DOI: 10.1021/j100329a007. Katsaounis, A. Recent developments and trends in the electrochemical promotion of catalysis (EPOC). *J. Appl. Electrochem.* **2010**, *40* (5), 885-902. DOI: 10.1007/s10800-009-9938-7. Imbihl, R. Electrochemical promotion of catalytic reactions. *Prog. Surf. Sci.* **2010**, *85* (5), 241-278. DOI: 10.1016/j.progsurf.2010.07.001.

(4) Giehr, A.; Maier, L.; Schunk, S. A.; Deutschmann, O. Thermodynamic Considerations on the Oxidation State of Co/γ-Al_2O_3 and Ni/γ-Al_2O_3 Catalysts under Dry and Steam Reforming Conditions. *ChemCatChem* **2018**, *10* (4), 751-757. DOI: 10.1002/cctc.201701376. Pakhare, D.;

Spivey, J. A review of dry (CO_2) reforming of methane over noble metal catalysts. *Chem. Soc. Rev.* **2014**, *43* (22), 7813-7837. DOI: 10.1039/C3CS60395D.

(5) Degerman, D.; Lömker, P.; Goodwin, C. M.; Shipilin, M.; García-Martínez, F.; Schlueter, C.; Nilsson, A.; Amann, P. State of the Surface During CO Hydrogenation over Ni(111) and Ni(211) Probed by Operando X-ray Photoelectron Spectroscopy. *J. Phys. Chem. C* **2023**, *127* (8), 4021-4032. DOI: 10.1021/acs.jpcc.2c07650.

(6) Chen, Y.; Zhang, Y.; Lin, Y.; Yang, Z.; Su, D.; Han, M.; Chen, F. Direct-methane solid oxide fuel cells with hierarchically porous Ni-based anode deposited with nanocatalyst layer. *Nano Energy* **2014**, *10*, 1-9. DOI: 10.1016/j.nanoen.2014.08.016. Qu, J.; Wang, W.; Chen, Y.; Deng, X.; Shao, Z. Stable direct-methane solid oxide fuel cells with calcium-oxide-modified nickel-based anodes operating at reduced temperatures. *Appl. Energy* **2016**, *164*, 563-571. DOI: 10.1016/j.apenergy.2015.12.014.

(7) Song, K.; Lu, M.; Xu, S.; Chen, C.; Zhan, Y.; Li, D.; Au, C.; Jiang, L.; Tomishige, K. Effect of alloy composition on catalytic performance and coke-resistance property of Ni-Cu/Mg(Al)O catalysts for dry reforming of methane. *Appl. Catal. B* **2018**, *239*, 324-333. DOI: 10.1016/j.apcatb.2018.08.023.

(8) Zambaldi, P.; Haug, L.; Penner, S.; Klötzer, B. Dry Reforming of Methane on NiCu and NiPd Model Systems: Optimization of Carbon Chemistry. *Catalysts* **2022**, *12* (3). DOI: 10.3390/catal12030311.

(9) Lee, G.-J.; Lee, J.-H.; Lee, D.; Park, K.-I.; Jeong, C. K.; Park, J.-J.; Lee, M.-K. Synthesis and characterization of carbon-coated Cu-Ni alloy nanoparticles and their application in conductive films. *Appl. Surf. Sci.* **2021**, *566*, 150672. DOI: 10.1016/j.apsusc.2021.150672.

(10) Luyten, L. J. M.; Von Eck, M.; Von Grondelle, J.; Von Hooff, J. H. C. Hydrogenation of carbon monoxide over silica supported nickel-copper and ruthenium-copper catalysts. *J. Phys.*

Chem. **1978**, *82* (18), 2000-2002. DOI: 10.1021/j100507a010. Hatta, A. H.; Jalil, A. A.; Hassan, N. S.; Hamid, M. Y. S.; Rahman, A. F. A.; Teh, L. P.; Prasetyoko, D. A review on recent bimetallic catalyst development for synthetic natural gas production via CO methanation. *Int. J. Hydrogen Energy* **2022**, *47* (72), 30981-31002. DOI: 10.1016/j.ijhydene.2021.10.213.

(11) Tsiotsias, A. I.; Charisiou, N. D.; Yentekakis, I. V.; Goula, M. A. Bimetallic Ni-Based Catalysts for CO_2 Methanation: A Review. *Nanomaterials* **2021**, *11* (1). DOI: 10.3390/nano11010028.

(12) Schmider, D.; Maier, L.; Deutschmann, O. Reaction Kinetics of CO and CO_2 Methanation over Nickel. *Industrial & Engineering Chemistry Research* **2021**, *60* (16), 5792-5805. DOI: 10.1021/acs.iecr.1c00389. WENSHENG, X.; HAIYOU, W.; HUILIN, W.; QIANER, Z. An energetics study on syngas($CO+H_2$) methanation reaction on Ni, Cu and Ni-Cu alloy surfaces by bond-order conservation model. *Acta Chim. Sinica* **1998**, *56* (8), 773-779.

(13) Luo, Y.; Li, W.; Shi, Y.; Ye, X.; Wang, S.; Cai, N. Methane Synthesis Characteristics of H_2O/CO_2 Co-Electrolysis in Tubular Solid Oxide Electrolysis Cells. *ECS Transactions* **2015**, *68* (1), 3465. DOI: 10.1149/06801.3465ecst.

(14) Fleig, J.; Baumann, F. S.; Brichzin, V.; Kim, H. R.; Jamnik, J.; Cristiani, G.; Habermeier, H. U.; Maier, J. Thin Film Microelectrodes in SOFC Electrode Research. *Fuel Cells* **2006**, *6* (3-4), 284-292. DOI: 10.1002/fuce.200500209 (acccessed 2023/03/23).

(15) Powell, C. J.; Jablonski, A.; Naumkin, A.; Kraut-Vass, A.; Conny, J. M.; Rumble, J. R. NIST data resources for surface analysis by X-ray photoelectron spectroscopy and Auger electron spectroscopy. In *Journal of Electron Spectroscopy and Related Phenomena*, 2001; Vol. 114, pp 1097-1102. Biesinger, M. C. Accessing the robustness of adventitious carbon for charge referencing (correction) purposes in XPS analysis: Insights from a multi-user facility data review. *Appl. Surf. Sci.* **2022**, *597*, 153681. DOI: 10.1016/j.apsusc.2022.153681.

(16) Zegkinoglou, I.; Pielsticker, L.; Han, Z.-K.; Divins, N. J.; Kordus, D.; Chen, Y.-T.; Escudero, C.; Pérez-Dieste, V.; Zhu, B.; Gao, Y.; et al. Surface Segregation in CuNi Nanoparticle Catalysts During CO2 Hydrogenation: The Role of CO in the Reactant Mixture. *The Journal of Physical Chemistry C* **2019**, *123* (13), 8421-8428. DOI: 10.1021/acs.jpcc.8b09912.

(17) Linstrom, P. NIST Chemistry WebBook, NIST Standard Reference Database 69. **1997**. DOI: 10.18434/T4D303.